PAPER

Serpentine-pattern effects on the biaxial stretching of percolative graphene nanoflake films

To cite this article: Sungwoo Chun *et al* 2020 *Nanotechnology* **31** 085303

IOP Publishing Nanotechnology
Nanotechnology 31 (2020) 085303 (9pp) https://doi.org/10.1088/1361-6528/ab5419

Serpentine-pattern effects on the biaxial stretching of percolative graphene nanoflake films

Sungwoo Chun[1,2], Sung Beom Cho[3], Wonkyeong Son[4], Younghoon Kim[4], Hachul Jung[5], Young-Jin Kim[5] and Changsoon Choi[4]

[1] Department SKKU Advanced Institute of Nanotechnology (SAINT), Sungkyunkwan University (SKKU), Gyeonggi-do 16419, Republic of Korea
[2] School of Chemical Engineering, Sungkyunkwan University, Suwon, Gyeonggi-do 16419, Republic of Korea
[3] Virtual Engineering Center, Korea Institute of Ceramic Engineering and Technology (KICET), Jinju-si, Gyeongsangnam-do 52851, Republic of Korea
[4] Division of Energy Technology, DGIST, Daegu 42988, Republic of Korea
[5] Medical Device Development Center, Osong Medical Innovation Foundation, Cheongju, Chungbuk 28160, Republic of Korea

E-mail: cschoi@dgist.ac.kr

Received 24 July 2019, revised 2 October 2019
Accepted for publication 4 November 2019
Published 26 November 2019

Abstract

Stretchable strain sensors based on percolative arrangements of conducting nanoparticles are essential tools in stretchable electronics and have achieved outstanding performance. Introducing serpentine patterns for strain-sensing materials is a very effective method for enhancing stretchability with a quantified structural resistance through a simple, reliable, and facile approach. Here, we investigate serpentine-pattern effects in the electrical responses to biaxial stretching for percolative graphene-nanoparticle films. Graphene nanoplatelet films are applied to a stretchable substrate using a facile spray-coating technique, for a variety of serpentine pattern shapes, aspect ratios, pattern frequencies, and number of coatings. The electrical responses after applying biaxial stretching (*x*-axis and *y*-axis) are measured and analyzed for comparison. The serpentine patterns that would be suitable for stretchable electrodes, sensitive sensors, and highly stretchable sensors are then identified. This work demonstrates the advantage of using serpentine patterns for stretchable strain sensors and offers guidelines for selecting suitable pattern types for strain sensors in stretchable-electronics applications.

Supplementary material for this article is available online

Keywords: serpentine, strain sensors, graphene, graphene nanoflakes, graphene sensors

(Some figures may appear in colour only in the online journal)

1. Introduction

Stretchable electronics has attracted significant interest for making next-generation electronic devices and systems for application in fields such as health care monitoring, human motion detection, electronic skin, prosthetics, soft robotics, Self-healing devices and medical applications [1–5]. Strain sensors are an essential component in realizing stretchable electronics and require high sensitivity and stretchability in addition to being ultra-thin, lightweight, adhesive, and deformable for wearability and bending. Much effort has been devoted to developing strain sensors that satisfy these requirements by the introduction of various types of sensing materials and their micro/nano structures [6–13]. Ultimately,

the outstanding sensor performances in sensitivity, stretchability, stability, and reversibility have mostly been made by conductive nanoparticle-based percolative systems [14, 15]. Many related theoretical and experimental results have been regularly reported [14–17,] and various types of applications to wearable electronic-sensor systems have been demonstrated [18, 19]. Among the sensing materials used, those based on graphene-based nanoparticles (e.g. graphene flakes, graphene nanoplatelets (GNP), graphene oxide, and reduced graphene oxide) are highly promising because of their extraordinary mechanical, chemical, and electrical properties [20]. In particular, they have been shown to be cheap, mass-producible, and easy to prepare because they involve facile-solution-based processes. In fact, graphene-based nanoparticles offer significant improvements in sensitivity and stretchability when compared to several-layer graphene-film-based strain sensors [21, 22]. For example, Hempel *et al* demonstrated that strain gauges based on layered percolative films of graphene flakes can achieve gauge factors (GFs) exceeding 150 through the morphology-dependent resistance of graphene film [23]. Recently, Jeong *et al* reported a stretchability of over 70% strain and a GF in the range of 15–29 using a fragmentized graphene-foam strain sensor [24]. However, stretchability sufficient to cover all application fields for strain sensors in stretchable electronics is yet to be achieved.

Introducing unusual architectures such as serpentine-shaped patterns, surface wrinkles, and 3D foam structures has been proposed as a way to improve stretchability [12, 25–28]. After wrinkling the morphology of graphene film formed on elastic substrates, the stretchability was found to be greatly enhanced [26, 27]. 3D graphene foams with porous architectures were fabricated by using facile techniques and were found to increase stretchability and flexibility [28]. However, these methods require complex processes, and reproducibility is relatively difficult, with facile and reliable approaches being preferred. However, forming serpentine patterns of strain-sensing materials on an elastic substrate using well-supported patterning techniques is a very facile and effective method because it alone enhances the stretchability with a quantified structural resistance. Moreover, the method can easily be applied to a wide variety of materials and structures. Although this technique is very effective for enhancing the stretchability without limitations on materials and the fabricating process, few studies that investigate serpentine-pattern effects on strain-sensing performance have been performed. The combination of a percolative GNP material and a serpentine structure can then be utilized in a variety of applications of wearable and attachable electronic sensor system that requires high stretchability.

To address this, we have investigated the effects of different serpentine patterns in percolative graphene films in terms of the electrical response to biaxial stretching. Graphene nanoflakes were applied to a stretchable ecoflex substrate using a facile spray-coating technique for a variety of serpentine pattern shapes, aspect ratios, pattern frequencies, and number of coatings. After stretching on each axis independently, the electrical responses of the films were measured, and the results analyzed. We believe that our approach suggests appropriate design rules for particle-based strain sensors, thereby opening the way for applications of strain sensors suited to the characteristics of stretchable electronics in various fields.

2. Experimental details

2.1. Fabrication of serpentine-patterned strain sensors

GNP were purchased from the graphene supermarket corporation. The thickness of each individual flake is $<\sim 3$ monolayers and the lateral flake size is ~ 10 μm with surface area of 510 $m^2 g^{-1}$. The GNP particles are vigorously mixed to form suspensions in chloroform solvent. Sonication is then applied using a sonication bath for 3 h to obtain well-dispersed GNP suspension. The suspension is then stirred with a magnetic bar (1 h at 400 rpm). The GNP suspension was coated on the ecoflex substrate by the spray coating method using different stencil masks. The diameter of the spray nozzle is 500 μm, and the spraying rate was 0.04 ml min^{-1}. The distance between the nozzle and the substrate was $\sim$15 cm. Spray deposition was performed by heating the substrates using a hot plate every 30 s at 150 °C. After assembling the thin ecoflex passivation layer ($\sim$100 μm thickness) onto the GNP film, the sensor devices were finally completed with the casting of liquid ecoflex layer and followed the vacuum treatment (2 h) and baking (2 h at 100 °C) processes.

2.2. Characterization

Optical microscope (Nikon ME600L) and field-emission scanning electron microscopy (Hitachi S-4800) were used for the optical images for the sensor device. Raman spectrometer (NRS-3100) with 532 nm of excitation wavelength was used for characterizing the GNP film. Conductivities of the GNP films depending on the numbers of spray coating were calculated by measured sheet resistance using a 4-point probe. For the stretching tests, the samples were equipped on home-made stretching stage with micro-position controller whose resolution is $\sim$7 μm. The NI precision system SMU (PXIe-4139) and sourcemeter (Keithley 2400) were used for the collections of electrical data with two contact channels of the samples.

3. Results and discussion

Figure 1(a) gives a schematic description of the process steps for fabricating percolative graphene strain sensors. Ecoflex was used as a substrate because of its excellent intrinsic stretchability (up to $\sim$300%). A GNP-based conductive film was selected for the strain-sensing material because of its individually formed percolative nanoparticles inside the film, as shown in figure 1(b). Such a percolative nanoparticle distribution enables sensitive and reversible detection of tensile

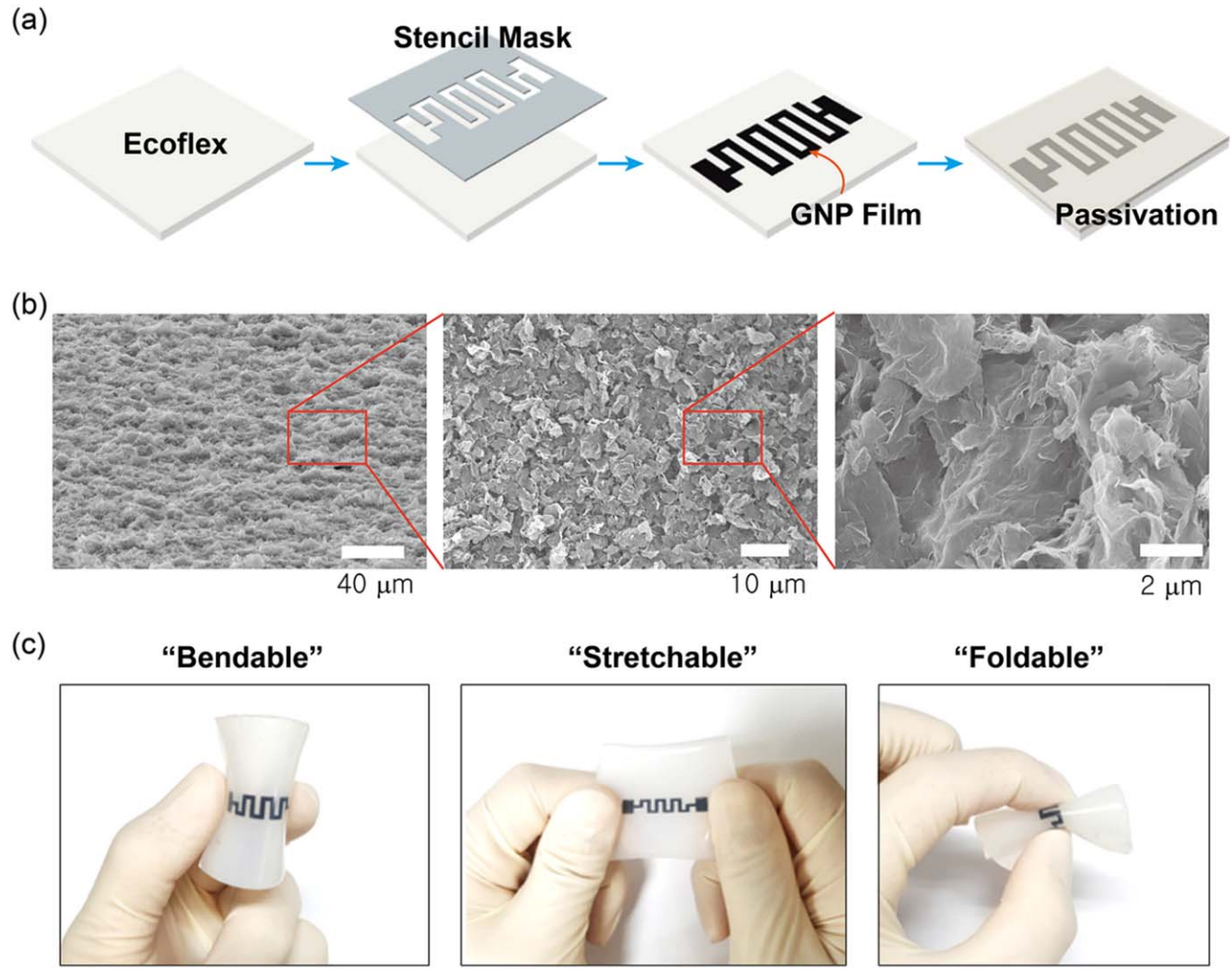

Figure 1. Percolative graphene nanoflake-based strain sensors. (a) Schematic description of process steps for fabricating percolative graphene strain sensors. A GNP suspension dispersed in chloroform was deposited on the ecoflex by spray coating using a stencil mask, followed by passivation with PDMS. (b) SEM images showing morphological distributions of the GNP nanoparticles. The particles are closely interacting mechanically and electrically with a percolative distribution. (c) Flexibility of the completed graphene strain sensor. It can be bent, stretched, and folded easily and robustly.

strain caused by variation in the physical contact areas between the GNP particles according to the stretching deformation [21]. Using a stencil mask, the GNP suspension dispersed in chloroform was deposited on the ecoflex using a facile spray coating technique. After removing the mask, the film was treated with thermal baking at 100 °C to enable the dispersion solution to evaporate completely. After assembling a thin ecoflex (∼100 μm thickness) as a protecting layer for the GNP film, the strain sensors were finally completed with a casting of liquid ecoflex, followed by vacuum-treatment (2 h) and baking (2 h at 100 °C) processes. The noticeable Raman resonances of the GNP film were observed for the G band (1582 cm^{-1}), the 2D band (2681 cm^{-1}), and the D band (1352 cm^{-1}), similar to those of a typical single-layer graphene film, but their intensities indicated that the percolative GNP nanopowder were multilayered graphene that included many spatial vacancies (see supplementary information (SI) figure S1 is available online at stacks.iop.org/NANO/31/085303/mmedia for details). Figure 1(c) shows the completed GNP strain sensor. When using fully soft materials, the sensors can be bent, stretched, and folded.

The strain-sensing performance for the various serpentine-pattern shapes shown in figure 2 was investigated. The GNP film samples were coated 300 times using a concentration of 1.5 mg ml^{-1} at a flow rate of ∼10 ml min^{-1}. Figure 2(a) shows photographs for the different types of patterned GNP films. The patterning shapes were: (1) line pattern (total length: 16 mm, width: 1 mm), (2) rectangular-shaped serpentine pattern (total length: 40 mm, width: 1 mm), (3) round-shaped serpentine pattern (total length: 35 mm, width: 1 mm), and (4) triangle-shaped serpentine pattern (total length: 30.5 mm, width: 1 mm), where the 'total length' excluded both electrodes. The biaxial tensile strains (for both *x*- and *y*-axes) were independently applied to an individual strain sensor with a strain resolution of 10% in the sample plane, and the electrical responses were measured via the GNP film electrodes. The GNP film width for the electrodes is several times wider than that for the strain-sensing channel

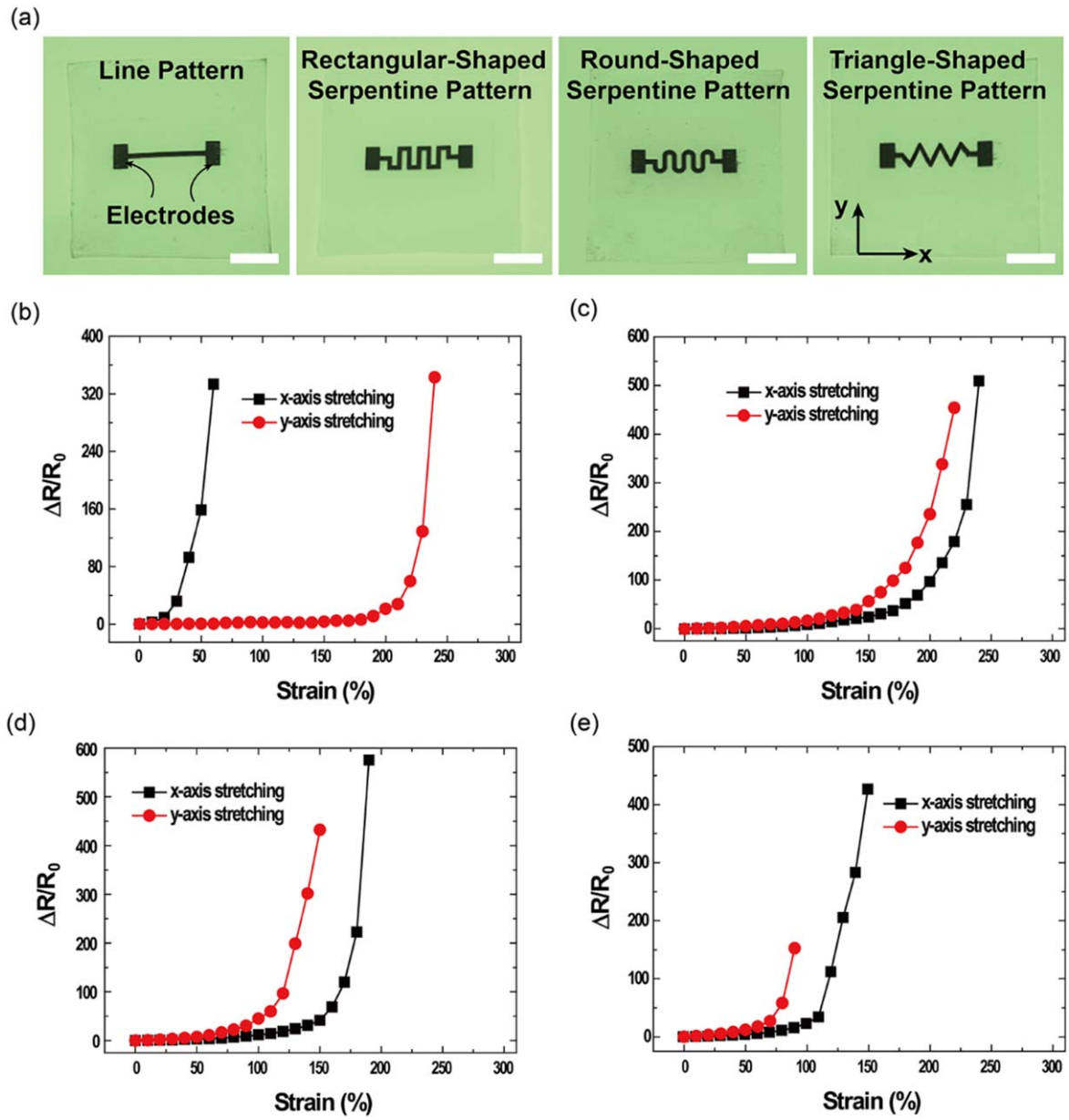

Figure 2. Strain-sensing performance for various serpentine pattern shapes. (a) Photographs for the different types of serpentine-patterned GNP films. The pattern shapes were: (1) line pattern (total length: 16 mm, width: 1 mm), (2) rectangular-shaped serpentine pattern (total length: 40 mm, width: 1 mm), (3) round-shaped serpentine pattern (total length: 35 mm, width: 1 mm), and (4) triangle-shaped serpentine pattern (total length: 30.5 mm, width: 1 mm), where the 'total length' excluded both electrodes. Electrical signals in response to biaxial tensile strains for both the *x*- and *y*-axes for samples of (b) line pattern, (c) rectangular shape, (d) round shape, and (e) triangle shape.

parts, in both x and y dimensions, to better withstand the strain. Furthermore, the electrodes were completely sealed by epoxy (Devcon Co.) to minimize strain effects. Figure 2(b) shows the electrical output signals in response to tensile strain for the line-pattern strain sensor. For x-axis stretching, the sensor shows a rapid increase in resistance with increasing strain. As a result, the sensor was electrically disconnected after a 60% strain. The GF is defined as GF $= (\Delta R/R_0)/\varepsilon$ with an assumption of linearity, where ΔR $(R–R_0)$ is the resistance change and ε is the applied strain. The applied strain is defined as an engineering strain of $(L–L_0)/L_0$ where L_0 and L is the length before and after stretching. In this figure, the GF is about 498 in the range of 0%–60% strain (a stretchability of 60%). Since the tensile strain is applied on the entire sample including underlying substrate (ecoflex: Young's modulus is ~30 kPa and Poisson ratio is 0.5), the sensor responses in resistance strongly reflect the relative mechanical behavior of the ecoflex with stretching. However, the sensor offers an improved stretchability (240%) in the y-axis, even though the GF is lower. This is attributed to widening the GNP film in the applied strain direction. The line-pattern GNP film with an x-axis strain can easily become disconnected because the current between the electrodes is easily isolated by a local disconnection caused by the narrow width (1 mm) of the GNP film. However, for a y-axis strain, there are many electrical paths inside the GNP film because of

Table 1. The gauge factor (GF) and stretchability for the graphene strain sensors with different shapes of serpentine pattern.

	Gauge factor (GF)		Stretchability	
Line pattern	*X* axis	~498(0%–60%)	*X* axis	60%
	Y axis	~3.1(0%–180%)	*Y* axis	240%
		~575(180%–240%)		
Rectangular-shaped	*X* axis	~16.3(0%–170%)	*X* axis	240%
		~702(170%–240%)		
Serpentine pattern	*Y* axis	~23(0%–130%)	*Y* axis	220%
		~485(130%–220%)		
Round-shaped	*X* axis	~19.8(0%–140%)	*X* axis	190%
		~1032(140%–190%)		
Serpentine pattern	*Y* axis	~41.5(0%–90%)	*Y* axis	150%
		~677(90%–150%)		
Triangle-shaped	*X* axis	~29.7(0%–100%)	*X* axis	150%
		~816(100%–150%)		
Serpentine pattern	*Y* axis	~37.6(0%–60%)	*Y* axis	90%
		~492(60%–90%)		

its length (16 mm) for electrons to move between the electrodes, even though the increasing strain gradually disconnects some of the pathways. This ultimately means that a GNP film with a larger dimension orthogonal to the strain direction is more resistant to the stretching force, thereby showing greater stretchability. This dimension-dependent electrical-response characteristic of the sensing film indicates that sensitivity and stretchability of percolation system-based strain sensors can be easily regulated by using simple dimension control. Moreover, the regulation of film dimensions in percolative GNP networks will enable their use as strain-insensitive electrodes for stretchable and wearable electronics. For the *y*-axis strain, the sensor actually shows small resistance change ($\Delta R/R_0 < 2$) up to a stretching of 140%.

These results demonstrate that the electromechanical sensing properties of particle-based strain sensors can be simply regulated by controlling the dimensions of percolative sensing films via simple line shapes. However, the response characteristics are so different that nonlinearities will induce extreme differences in GF across the stretching range. To address this and to further increase stretchability, we introduce serpentine patterns for the GNP film. It is well known that serpentine-pattern sensing films provide improved stretchability in tensile strain because the patterns spread the stretching force across the film [12, 25, 29]. To understand the geometric effect of the strain sensors, we first performed finite element analysis as implemented in COMSOL Multiphysics. Figure S2 shows the local region where von Mises stress distribution is concentrated when the various shape of GNP is under 20% of tensile strain over the parallel direction of electrodes. We found out the line-pattern suffers huge stress over the entire region compared to the other-shape patterns, as shown in figure S2(a). This geometry cannot include bending deformation over perpendicular direction, thereby it should suffer under tensile stress directly. This stress-localized region introduces the resistivity increases. When the carbon–carbon bonds of graphene are stretched under the tensile stress, the bandgap of the graphene opens that leads to the increase of the resistivity [30]. The tensile stress applied near the grain boundaries also shows similar bandgap opening [31]. Thereby, the stress-localized region is expected to have a local band gap, which contributes to the resistivity increase. On the other hands, the triangle-shaped, round-shaped, and rectangular-shaped GNP films have more relieved stress distribution except some of the localized regions near the corners (figures S2(b)–(d)). Thereby the relieved region behaves like 'conductive path'. For the triangle-shaped GNP film, the conductive path is interrupted by the localized stress at the corners. On the other hands, the round-shaped and rectangular-shaped GNP film has 'conductive path'. In particular, the rectangular-shaped one has wider channel than the round-shaped one. Thereby the strain-absorbing trends are rectangular-shaped, rounded-shaped, triangular-shaped, and line-shaped GNP channel in descending order. This trend is consistent with the experimental observation of drastic resistivity change in figure 2. We also tested different case of aspect ratio and serpentine frequency as shown in figures S2(e), (f). As aspect ratio increases, the stress is more dispersed due to increased length along the perpendicular direction of the channel. When the serpentine frequency is decreased, more stress is localized near the edge thereby resistivity increases rapidly.

Experimentally, we constructed a GNP film with a rectangular-shaped serpentine pattern. The direct distance between the electrodes was the same as that for the line-pattern case (16 mm), but the distance along the film was 40 mm (i.e. more than two times longer). The width was 1 mm, as for the line-pattern case. Figure 2(c) shows the electrical output signals in response to tensile strain for this strain sensor. For the *x*-axis stretching, the sensor shows two distinct behaviors: a pattern expansion-dominant region and a GNP-film stretching-dominant region. For the initial pattern expansion region, the serpentine pattern mostly absorbs the stretching force, giving a low GF of 0–20 for a strain range of 0%–170%. This is attributed to both the stretching effect of GNP sheets inside the film (increasing the resistance) and the

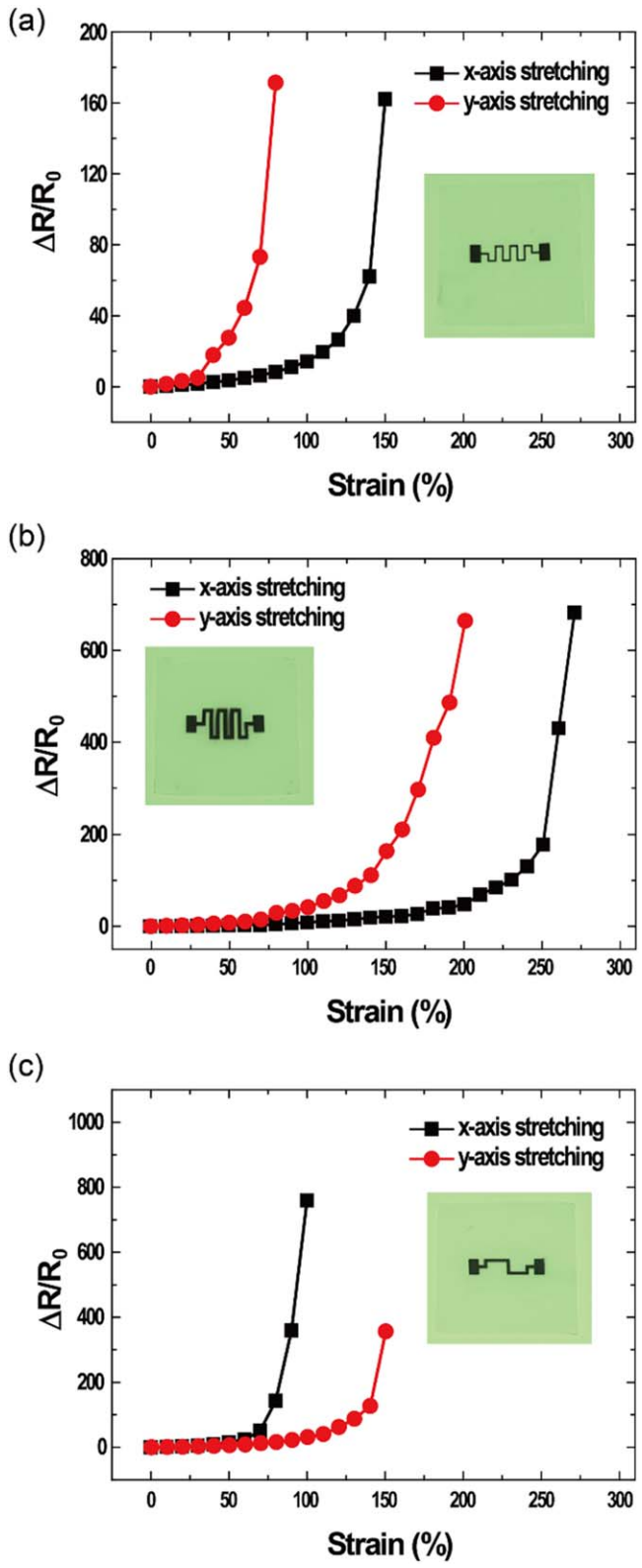

Figure 3. Width, aspect-ratio, and frequency effects of the serpentine patterns on strain sensing performance. Electrical signals in response to biaxial tensile strains in both the *x*- and *y*-axes for variations in rectangular-shaped serpentine patterns: (a) decreased width (from 1 to 0.5 mm), (b) increased aspect ratio (from 5/3 to 3), and (c) decreased serpentine frequency (from length = 40 to 24 mm).

improved mobility effect of electrons by spreading the serpentine pattern (decreasing the resistance). In this region, the effect of the applied tensile strain is mainly to flatten the serpentine shape, although the total resistance is slightly increased. In the *x*-axis stretching, sensitivity in GF depends on the geometry of patterns. It is noted that stretching of any film induces compression simultaneously along the vertical direction specified by the Poisson ration as an elastomer parameter. The resistance change is much dominant for the case where stretching is applied to the same direction of current path [12]. By contrast, above a strain of 170%, the sensor is directly subjected to the stretching effects of the GNP film. The resulting GF can then exceed 700, with a response characteristic in this range very similar to that of the line-pattern GNP film. Difference in resistance response from the line-patterned sensor comes from serpentine patterns (SI figure S3). For *y*-axis stretching, the sensor shows response characteristics similar to *x*-axis stretching. However, the mechanism is different from that for *x*-axis stretching. The resistance in *y*-axis stretching is mostly determined by the width of the GNP film in the longitudinal direction (parallel to the *y*-axis). However, the reason for the different response in this case is that the GNP film parallel to the *y*-axis is released by the GNP film parallel to the *x*-axis because elastic films induce compression along the vertical direction specified by the Poisson ratio as an elastic parameter. The GFs for the two behaviors with *y*-axis stretching were measured as 23 (0%–130%) and 485 (130%–220%). In the applications, we attempted stretchable strain sensors for detecting physical motions of human body. Figure S4 shows the detection in electrical resistance of bending motion of finger and knee.

The stretching-dependent electrical responses were then investigated for two other shapes of serpentine pattern. The round- and triangle-shaped serpentine-pattern strain sensors exhibit electromechanical behavior for *x*-axis stretching similar to that for the rectangular-shaped case, as shown in figures 2(d) and (e), respectively. The stretching range is only decreased because of the reduction in the total length of the GNP film to withstand the stretching force. The stretchability for pattern expansion is 140% for the round-shaped case and 100% for the triangle-shaped case, respectively. Note that the differences in stretchability between *x*- and *y*-axis stretching are large *r* in the round- and triangle-shaped cases than in the rectangular-shaped case. This is because the round and triangle patterns have smaller stretching forces to be spread, given their small structural resistance, in addition to showing smaller compensation in the GNP film parallel to the *y*-axis because of the compression by Poisson ratio of the elastic GNP film parallel to the *x*-axis. The GF and stretchability for GNP strain sensor with different shapes of serpentine pattern is summarized in table 1. The table offers guidelines for selecting suitable pattern types for strain sensors in stretchable-electronics applications. The GF and stretchability of our graphene strain sensor is highly comparable to previously reported graphene-based strain sensors: piezoresistive

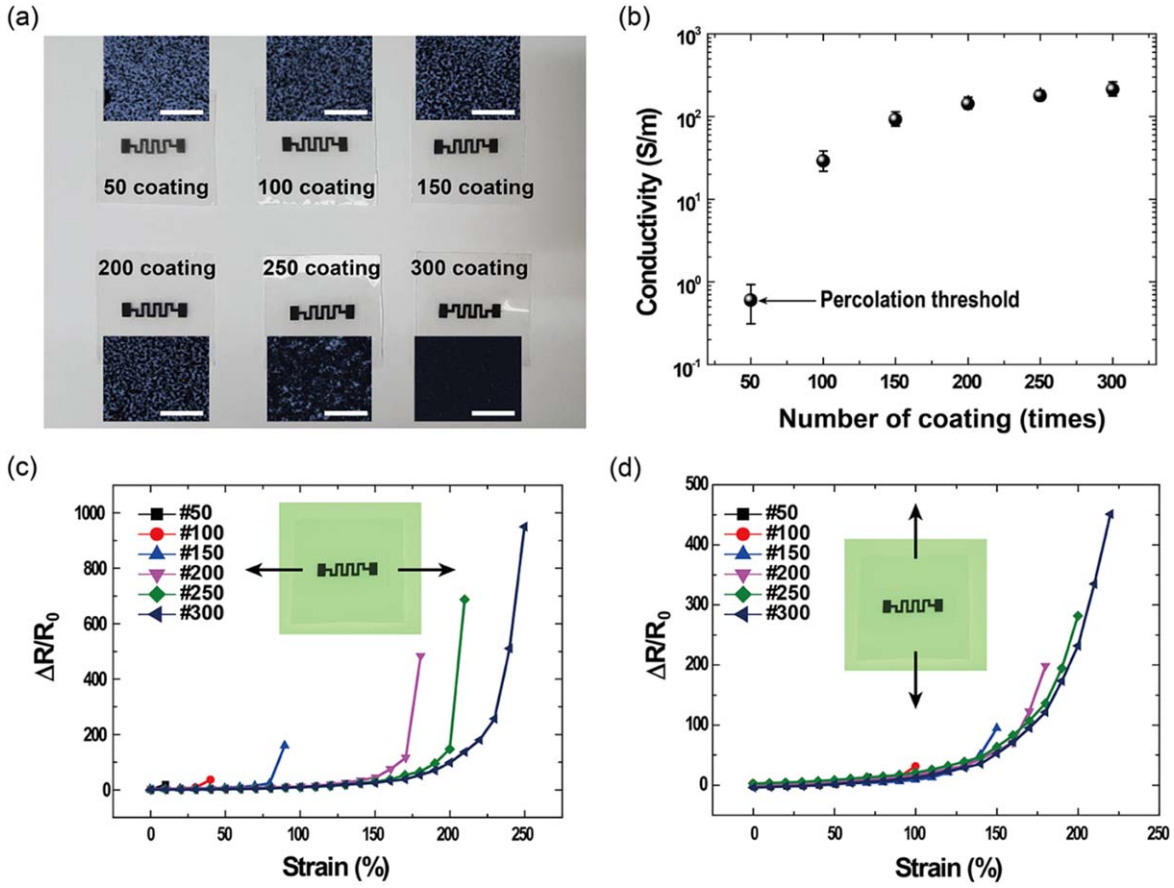

Figure 4. Serpentine-patterned graphene film with various coating densities. (a) Photographs and optical images of rectangular-shaped serpentine pattern GNP films with different coating densities, as determined by the number of spray coatings (50–300). The GNP concentration was 1.5 mg ml^{-1}, and the flow rate for the spray coating was ~10 ml min^{-1}. (b) Electrical conductivity of the GNP film as a function of the number of spray coatings. (c) Electrical responses of the various GNP films to tensile strain in the *x*-axis. (d) Electrical responses for a *y*-axis tensile strain.

nanographene film-based strain sensor (GF: 300, stretchability: 0.37%), chemical vapor deposition graphene strain sensor (GF: 14, stretchability: 7.1%), laser scribing-based graphene strain sensor (GF: 9.49, stretchability: 10%), fragmentized graphene foam-based graphene strain sensor (GF: 15–29, stretchability: 70%), graphene/glycerol synergistic conductive network strain sensor (GF: 25.2, stretchability: 300%) [24, 32–35].

The effects of variations in width, aspect ratio, and frequency on strain-sensing performance for serpentine patterns were investigated, as shown in figure 3. For these experiments, only the rectangular-shaped serpentine pattern was used. With a decreased width (from 1 to 0.5 mm), figure 3(a) shows that the stretchability for the pattern expansion-dominant region decreased to ~90% for *x*-axis stretching, compared with the original rectangular-shaped serpentine pattern (see figure 2(c)). The thinner the width of the serpentine pattern, the faster the resistance increases, indicating low stretchability. It offers lower stretchability for *y*-axis stretching because of both a thinner width and smaller compensation effects. Figure 3(b) shows that the increased pattern length (from 40 to 64 mm) accompanying an increased aspect ratio (from 5/3 to 3) requires more *x*-axis stretching to expand the serpentine pattern than the original pattern shown in figure 2(c), giving a wider pattern-expansion-dominant region (~190%). However, for *y*-axis stretching, the longer *y*-axis length does not affect the electrical response significantly. A low-frequency (total length: 24 mm, width: 1 mm) serpentine pattern exhibits low stretchability for both *x*- and *y*-axis stretching, as shown in figure 3(c).

In a final experiment, the coating density for the GNP film was varied, as determined by the number of spray coatings. Figure 4(a) shows photographs and optical images for rectangular-shaped serpentine pattern GNP films with different coating densities. The GNP concentration was 1.5 mg ml^{-1}, and the flow rate for the spray coating was ~10 ml min^{-1}. The number of spray coatings varied from 50 to 300 (see SI figure S5). An #50 coating is close to the film threshold and a GNP film with a #300 coating has microscopic cracks inside caused by coating instability (see SI figure S6). With a denser coating, neighboring GNP sheets interact more closely, both physically and electrically, and in both horizontal and vertical directions. Figure 4(b) shows the electrical conductivity of GNP films for various densities of spray coating. The conductivities range from 6×10^{-1} to 2.1×10^{2} S m^{-1}. The initial resistance has a decisive influence on the stretchability of the strain sensor because the

electrical disconnection of GNP sheets decides the stretching limit.

The effects on strain-sensing performance of varying the percolative film density for a serpentine pattern were then measured. Rectangular-shaped serpentine-pattern-based strain sensors were stretched independently in the *x*- and *y*-axes. Figures 4(c) and (d) show the piezoresistive responses of the strain sensors to *x*-axis and *y*-axis stretching, respectively, for various GNP film coating densities. Without external strain, the resistance (R_0) of the percolative GNP sensor was determined by natural random networks of as-coated GNP sheets. The sheets are spatially distributed by overlapping within a certain distance, exhibiting electrical resistance depending on physical interaction between the GNP sheets. The applied tensile strains increase the resistance (R) of the sensors due to a change in film morphology as electrical interactions between the sheets are gradually decreased with the increase in the distance between the sheets. Eventually, the resulting resistance ($\Delta R = R–R_0$) is mostly caused by the changes in the spatial distance for the interaction. In a percolative modeling of current through a network of randomly positioned circular flakes, the contact resistance of overlapping flakes is determined by calculating their contact area. The resistance change for the flakes network is thus calculated by solving the Kirchhoff equations. The neighboring flakes can lose their contact area under tensile strains, and the local percolation pathways are broken, thus making sensitivity large. The lower coating density, the less percolation pathways are made, making them more sensitive but less stretchable. As expected, the stretchability is higher for higher-density GNP film sensors with respect to both *x*- and *y*-axis stretching. Conversely, the GF is high for a low-density GNP film sensor, which is closer to the threshold. These response characteristics indicate how the electromechanical performance of percolative GNP film-based strain sensors can be controlled through simple regulation of the film density. This approach can be applied in a variety of application fields that require specific sensitivities and stretchability values.

4. Conclusions

In summary, we report on our investigations into stretchable strain sensors based on percolative graphene nanoflakes that were fabricated with serpentine-shaped patterns on an ecoflex substrate. Fabrication involved simple spray coating through a stencil mask. By varying the shapes, aspect ratios, pattern frequencies, and number of coating layers for the serpentine patterns, the range of electrical responses under biaxial stretching were investigated. Depending on the geometrical shape and film density adopted, the particle-based strain sensor can be used for stretchable electrodes, sensitive strain sensors, and stretchable strain sensors. Based on these demonstrations, we believe that our work will be an important milestone for strain-sensor applications in stretchable electronics.

Acknowledgments

This work was supported by the Basic Science Research Program (NRF-2017R1A6A3A04004987, 2018R1A6A3A01011866 and 2019R1F1A1058554) through the National Research Foundation of Korea funded by the Ministry of Education, and the DIGIST R&D Program (18-NT-02) funded by Ministry of Science, ICT and Future Planning of Korea. This work was supported by the National Research Foundation of Korea (NRF) Grant funded by the Korean Government (MSIP) Grant No. (NRF-2016R1A5A1921651).

ORCID iDs

Sungwoo Chun https://orcid.org/0000-0002-8533-0388
Hachul Jung https://orcid.org/0000-0001-9437-8618
Changsoon Choi https://orcid.org/0000-0003-4456-4548

References

[1] Rogers J A, Someya T and Huang Y 2010 *Science* **327** 1603–7
[2] Ramuz M, Tee B C K, Tok J B H and Bao Z 2012 *Adv. Mater.* **24** 3223–7
[3] Jang H, Park Y J, Chen X, Das T, Kim M S and Ahn J H 2016 *Adv. Mater.* **28** 4148–4202.
[4] Liu Y, Pharr M and Salvatore G A 2017 *ACS Nano* **11** 9614–35
[5] Wu J *et al* 2018 *ACS Appl. Mater. Interfaces* **10** 19097–105
[6] Lipomi D J, Vosgueritchian M, Tee B C K, Hellstrom S L, Lee J A, Fox C H and Bao Z 2011 *Nat. Nanotechnol.* **6** 788–92
[7] Yan C, Wang J, Kang W, Cui M, Wang X, Foo C Y, Chee K J and Lee P S 2013 *Adv. Mater.* **26** 2022–7
[8] Amjadi M, Kyung K U, Park I and Sitti M 2016 *Adv. Funct. Mater.* **26** 1678–98
[9] Frutiger A, Muth J T, Vogt D M, Menguc Y, Campo A, Valentine A D, Walsh C J and Lewis J A 2015 *Adv. Mater.* **27** 2440–6
[10] Shi J *et al* 2016 *Adv. Funct. Mater.* **26** 2078–84
[11] Harada S, Honda W, Arie T, Akita S and Takei K 2014 *ACS Nano* **8** 3921–7
[12] Chun S, Choi Y and Park W 2017 *Carbon* **116** 753–9
[13] Wu J, Wu Z, Lu X, Han S, Yang B-R, Gui X, Tao K, Miao J and Liu C 2019 *ACS Appl. Mater. Interfaces* **11** 9405–14
[14] Hempel M, Nezich D, Kong J and Hofmann M 2012 *Nano Lett.* **12** 5714–8
[15] Ryu S, Lee P, Chou J B, Xu R, Zhao R, Hart A J and Kim S G 2015 *ACS Nano* **9** 5929–36
[16] Kyrylyuk A V, Hermant M C, Schilling T, Klumperman B, Koning C E and van der Schoot P 2011 *Nat. Nanotechnol.* **6** 364–9
[17] Saberi A A 2015 *Phys. Rep.* **578** 1–32
[18] Shi G, Zhao Z, Pai J H, Lee I, Zhang L, Stevenson C, Ishara K, Zhang R, Zhu H and Ma J 2016 *Adv. Funct. Mater.* **26** 7614–25
[19] Yin B, Wen Y, Hong T, Xie Z, Yuan G, Ji Q and Jia H 2017 *ACS Appl. Mater. Interfaces* **9** 32054–64
[20] Chabot V, Higgins D, Yu A, Xiao X, Chen Z and Zhang J 2014 *Energy Environ. Sci.* **7** 1564–96
[21] Bae S H, Lee Y, Sharma B K, Lee H J, Kim J H and Ahn J H 2013 *Carbon* **51** 236–42
[22] Fu X W *et al* 2011 *Appl. Phys. Lett.* **99** 213107
[23] Hempel M, Nezich D, Kong J and Hofmann M 2012 *Nano Lett.* **12** 5714–8

[24] Jeong Y R, Park H, Jin S W, Hong S Y, Lee S S and Ha J S 2015 *Adv. Funct. Mater.* **25** 4228–36
[25] Xu S *et al* 2013 *Nat. Commun.* **4** 1543
[26] Mu J, Hou C, Wang G, Wang X, Zhang Q, Li Y, Wang H and Zhu M 2016 *Adv. Mater.* **28** 9491–7
[27] Wang Y, Yang R, Shi Z, Zhang L, Shi D, Wang E and Zhang G 2011 *ACS Nano* **5** 3645–50
[28] Kuang J, Liu L, Gao Y, Zhou D, Chen Z, Han B and Zhang Z 2013 *Nanoscale* **5** 12171–7
[29] Rahimi R, Ochoa M, Tamayol A, Khalili S, Khademhosseini A and Ziaie B 2017 *ACS Appl. Mater. Interfaces* **9** 9015–23
[30] Gui G, Li J and Zhong J 2008 *Phys. Rev.* B **78** 075435
[31] Nguyen V H, Hoang T X, Dollfus P and Charlier J-C 2016 *Nanoscale* **8** 11658–73
[32] Zhao J, He C, Yang R, Shi Z, Cheng M, Yang W, Xie G, Wang D, Shi D and Zhang G 2012 *Appl. Phys. Lett.* **101** 063112
[33] Bae S-H, Lee Y, Sharma B K, Lee H-J, Kim J-H and Ahn J-H 2013 *Carbon* **51** 236–42
[34] Tian H, Shu Y, Cui Y-L, Mi W-T, Yang Y, Xie D and Ren T-L 2014 *Nanoscale* **6** 699–705
[35] Liu C, Han S, Xu H, Wu J and Liu C 2018 *ACS Appl. Mater. Interfaces* **10** 31716–24